Biochemical and Biophysical Research Communications 478 (2016) 1694–1699

Contents lists available at ScienceDirect

Biochemical and Biophysical Research Communications

journal homepage: www.elsevier.com/locate/ybbrc

The development of a single molecule fluorescence standard and its application in estimating the stoichiometry of the nuclear pore complex

Hieng Chiong Tie [1], Viswanadh Madugula [1], Lei Lu*

School of Biological Sciences, Nanyang Technological University, 60 Nanyang Drive, 637551, Singapore

ARTICLE INFO

Article history:
Received 27 August 2016
Accepted 1 September 2016
Available online 6 September 2016

Keywords:
Stoichiometry
Single molecule
Nucleoporin
Nuclear pore complex
Fluorescence microscopy

ABSTRACT

We report here an image-based method to quantify the stoichiometry of diffraction-limited sub-cellular protein complexes *in vivo* under spinning disk confocal microscopy. A GFP single molecule fluorescence standard was first established by immobilizing His-tagged GFP molecules onto the glass surface via nickel nitrilotriacetic acid functionalized polyethylene glycol. When endogenous nucleoporins were knocked down and replaced by the exogenously expressed and knockdown-resistant GFP-nucleoporins, the stoichiometry of the nucleoporin was estimated by the ratio of its fluorescence intensity to that of the GFP single molecules. Our measured stoichiometry of Nup35, Nup93, Nup133 and Nup88 is 23, 18, 14 and 9 and there are possibly16 copies of Nup107-160 complex per nuclear pore complex.

1. Introduction

Proteins often dynamically assemble as complexes of certain stoichiometry for their proper molecular and cellular functions. Stoichiometry is important for our understanding of the structure and function of a protein complex. The subunit stoichiometry is conventionally assessed by biochemical approaches. For example, by using the purified or enriched nuclear pore complex (NPC), the stoichiometry of its subunits, called nucleoporins (Nups), has been empirically determined by gel blotting intensity or quantitative mass spectrometry [1–3]. There are however at least three disadvantages for the conventional bulk biochemical approach. First, the purification of an intact protein complex to homogeneity can be very challenging. Second, the ensemble-averaged stoichiometry is unable to reveal the individualities of protein complexes. Third, the quantification is conducted *in vitro* instead of in an *in vivo* cellular environment.

The availability of fluorescence proteins in conjunction with the advancement of microscopy has made it possible to directly assess the stoichiometry of protein complexes. One method is to directly count the number of discrete photobleaching steps (photobleaching method) [4]. However, as the stoichiometry increases to >5, it becomes technically challenging to unambiguously identify photobleaching steps, hence limiting this method to only small complexes on cell surfaces. The problem could be solved by adopting special microscopic techniques such as SPEED microscopy [5]. An alternative method is based on fluorescence intensity ratio (intensity method). To this end, a fluorescence standard of known stoichiometry must be first established. Next, the individual subunits of the protein complex are fluorescence-labeled and the subunit stoichiometry can be worked out by comparing the fluorescence intensity of the complex to that of the standard. Establishing the fluorescence intensity standard is the key to the success of this method. Viral-like particles (VLP) containing 120 copies of GFP-VP2 and bacterial homo-oligomeric complex of 10–24 subunits have been reported as standards for this purpose [6,7]. However, fluorescence-tagged subunits of these standards could be rendered non-fluorescent during preparation, storage or imaging. Since single molecules display all-or-none fluorescence, the fluorescence intensity of individual single molecules is not subject to the population decay. Hence, single molecules should make better fluorescence intensity standard. Here we describe a convenient method of obtaining the single molecule fluorescence standard by quantifying the intensity difference during single-step photobleaching. Using this standard, we systematically measured the stoichiometry of Nups in cultured mammalian cells.

NPCs are 8-fold rotational symmetry channels on the nuclear

* Corresponding author.
E-mail address: lulei@ntu.edu.sg (L. Lu).
[1] Equal contribution.

http://dx.doi.org/10.1016/j.bbrc.2016.09.005

envelope (NE) that serve as passages for bidirectional transport between the nucleus and cytosol [8]. With a molecular mass of ~120 MDa, the NPC is one of the largest proteinaceous complexes in a mammalian cell [9]. Despite its gigantic size, there are only ~30 types of Nups in the NPC. At the moment, the X-ray crystallographic structure of the NPC does not exist and the molecular architecture of the NPC is unknown. There are ongoing attempts in elucidating the structure of the NPC and tremendous progress has been made recently [10]. Stoichiometry has been the key information in building or evaluating structural models of the NPC. However the experimental results on the stoichiometry of the NPC are largely inconsistent. This could be reflected by the stoichiometry of Nup133, which is a key subunit of the core complex – Nup107-160 complex (Y-complex). By a biochemical approach, Cronshaw et al. estimated it to be 8 by gel staining [2]. On the other hand, by an imaging-based intensity method, Rabut and Finan et al. measured 25 and 32 copies of Nup133 per NPC, demonstrating that the stoichiometry of Nup133 is probably 32 [7,11]. This result is consistent with that from the integrative approach combining quantitative mass spectrometry, cryo-EM and crystallography [3,12–15]. However, by combining photobleaching with intensity approach, Mi and Schuster et al. reported 16 copies of Nup133 per NPC in yeast cells [5,16]. Therefore, there is a need to further verify or resolve these discrepancies by independent methods. Here, we report the estimation of the stoichiometry of the NPC by a single molecule based intensity method.

2. Materials and methods

2.1. Construction of DNA plasmids

Please see Supplementary material for details.

2.2. Tissue culture, transfection, knockdown, Western blot and antibodies

HeLa and HEK293 cells were cultured in DMEM supplemented with 10% fetal bovine serum at 37 °C in 5% CO_2 incubator. Transfection was conducted using Lipofectamine 2000 (Invitrogen) according to manufacturer's protocol. For knockdown experiments, HeLa cells were co-transfected with shRNA constructs in pSUPER.retro.puro vectors and GFP-Nup constructs (wild types or mutants). After 3 days, cells were either processed for immunofluorescence microscopy or lysed in 1xSDS sample buffer for Western blot analysis. Anti-β-tubulin (mouse monoclonal) (#sc5274) and anti-GFP (mouse monoclonal) (#sc9996) antibodies were purchased from Santa Cruz Biotechnology. HRP-conjugated goat anti-mouse IgG antibody was purchased from Bio-Rad. The quantification of Western blot bands was conducted in ImageJ (http://imagej.nih.gov/ij/).

2.3. Preparation of GFP single molecules on Ni-NTA-PEG-coated glass surface

A #1.5 Φ25 mm glass coverslip was first sequentially cleaned by NaOH and ethanol in a bath sonicator. After extensive rinse in water, the coverslip was dried in an oven. Next, the coverslip was placed on top of a drop of poly(L-lysine)-graft-poly(ethylene glycol) co-polymer (PEG, negative control) (Susos AG, #PLL(20)-g[3.5]-PEG2) or poly(L-lysine)-graft-poly(ethylene glycol) co-polymer with NTA end-functionalized PEG chains (NTA-PEG) (Susos AG, # PLL(20)-g[3.5]-PEG(3.4)-NTA) for 1.5 h at room temperature. After washing extensively with water, the coverslip was dried in a vacuum. The NTA group was loaded with nickel by incubating the coated glass surface with a drop of 50 mM $NiCl_2$ solution on the surface of Parafilm (Bemis) at room temperature for 2 h. After washing extensively with water, a chamber was assembled using PEG- or Ni-NTA-PEG-coated coverslip with the coated side up. Immerse the Ni-NTA-PEG-coated coverslip with PBS containing 5 mM imidazole at room temperature for 15 min to block Ni-NTA group. HEK293 cells were transfected to transiently express 6 × His-GFP. Cells were lysed in PBS buffer with 0.1% Triton X-100 and the resulting lysate was cleared by high speed centrifugation in a refrigerated table-top centrifuge. The coverslip was kept in dark for the following steps. The lysate was applied into the PEG- or Ni-NTA-PEG-coated coverslip chamber at room temperature. The density of 6 × His-GFP single molecules could be controlled by the dilution of the cell lysate and the incubation time. After washing with water, the coverslip was dried in a vacuum. A small amount of Tetraspeck fluorescence beads (Invitrogen) were applied to the center of the coverslip to aid in finding and focusing the coated surface. After the fluorescence bead slurry on the coverslip dried in the vacuum, the coverslip were mounted in Mowiol mounting medium, which contains 20% Mowiol 4-88 (EMD Merck), 9% glycerol, 109 mM Tris pH8.0 and 0.3% 1,4-diazabicyclo[2.2.2]octane (Sigma).

2.4. Imaging

GFP single molecules and nuclear pores were imaged under a spinning disk confocal microscope system comprising Olympus IX81 microscope (Olympus) equipped with an oil objective lens (100×, 1.45 NA), a piezo z-stage, Yokogawa CSU-X1 spinning head, an extra magnification lens and an EMCCD camera (Evolve; Photometrics). GFP fluorophores were excited by a 50 mW 488 nm solid state laser (Sapphire; Coherent), which was controlled by an acousto-optic tunable filter. The emission light of GFP was collected after it sequentially passed through a GFP dichroic mirror (Semrock, #Di01-T488) and a GFP long-pass emission filter (Semrock, #BLP01-488R) (mounted in the filter wheel of CSU-X1). The microscope system was controlled by Metamorph software (Molecular Devices). The pixel size was measured to be 67 nm by a micro-ruler (Geller MicroAnalytical Laboratory). The z-step of image stacks was 200 nm. The acousto-optic tunable filter was set as 80%. The gain of the EMCCD camera was 1 × . The digitizer used was 5 MHz with EM gain 700. The exposure time for GFP single molecules (t_a) and NPCs (t_b) ranged from 100 to 400 ms. After acquisition, NPC images were subjected to manipulation by multiplying them with a factor of t_a/t_b to normalize the difference in the exposure time (no image saturation was resulted).

2.5. Image analysis

Image analysis was performed in ImageJ. Only the central quadrant of the EMCCD image was used for quantitative analysis. For the 2D time-lapse of GFP single molecules, objects were manually selected using round ROIs with diameters of 7 pixels in the first frame of the time-lapse. The mean intensities within ROIs at each time point were acquired by ImageJ and subsequently exported to Excel. The mean intensity vs time was plotted in Excel and photobleaching time points were visually identified. Intensity traces fulfilling the following two criteria were selected for analysis: 1) displaying single-step intensity drop and 2) possessing more than 7 frame before and 10 frames after the photobleaching time point. The intensity of the GFP single molecule (I_{GFP}) is therefore calculated as the difference between the mean value before and after the photobleaching time point. For nuclear pore images, the 3 z-sections were visually examined to choose the best focused section. 7 × 7 square ROIs were manually selected similar to the analysis of GFP single molecules. An ImageJ macro was

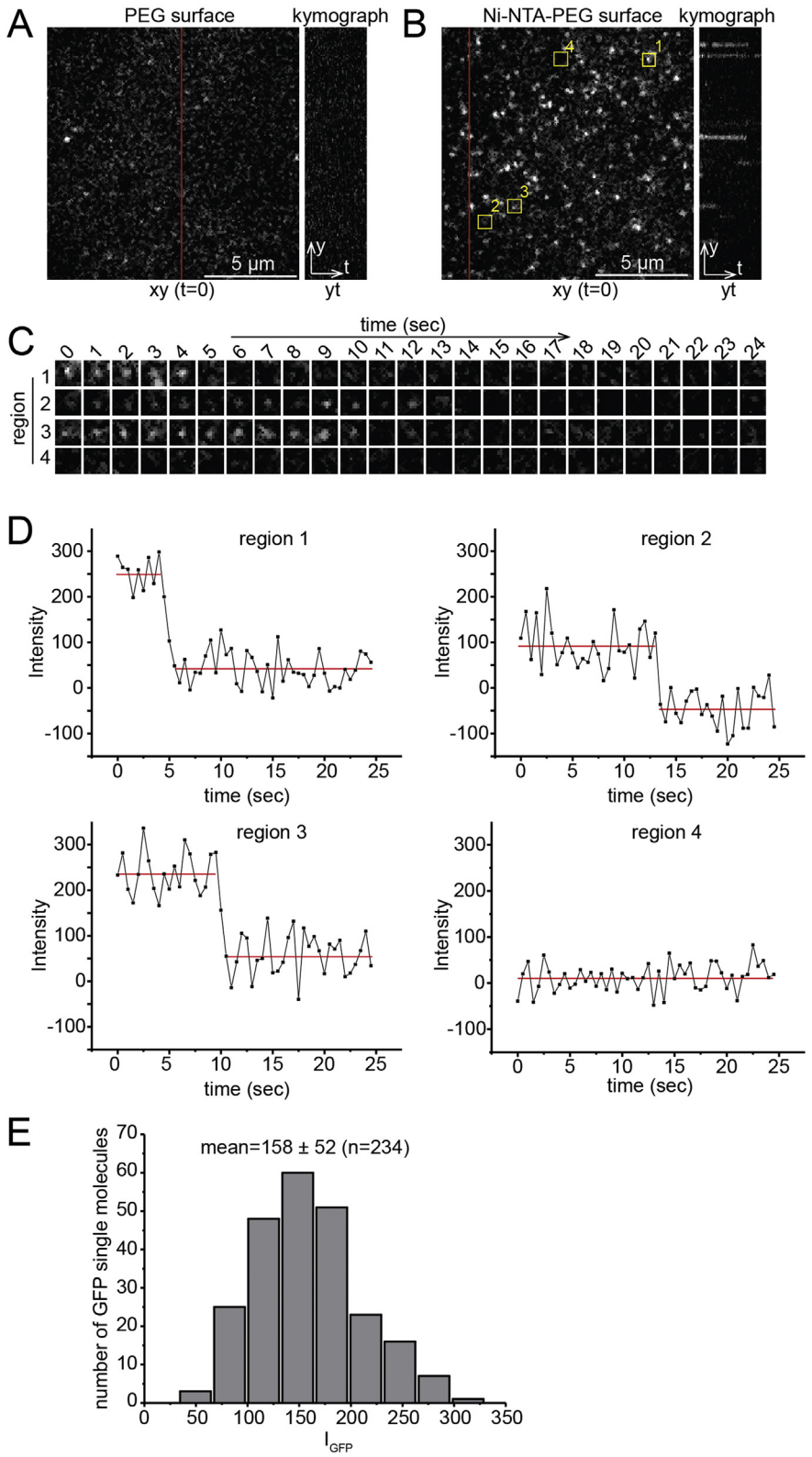

Fig. 1. Single GFP molecules as a fluorescence standard. (A, B) PEG- or Ni-NTA-PEG-coated glass coverslip incubated with cell lysate expressing 6 × His-GFP was imaged by a spinning disk confocal microscope as a 2D time-lapse. The left panel is the image of xy plane at t = 0. Scale bar, 5 μm. The right panel is the yt kymograph. The vertical red line denotes the x position of the kymograph. (C) Time-lapse series of selected regions (11 × 11 pixels) which are marked in (B). Region 1, 2 and 3 contain typical single GFP molecules. Region 4 shows a background control. (D) The mean intensity (within a round ROI with the diameter of 7 pixels) versus time traces for regions 1-4. (E) Histogram and statistics of single GFP molecules. Mean, standard error of the mean and n are denoted.

developed to automatically convert each 7 × 7 square ROI to a 7-pixel diameter round ROI and a concentric 9-pixel diameter round ROI. The mean intensities within the central and ring ROIs were acquired at each time point and the intensity of the GFP-Nup

(I_{Nup}) is therefore calculated as the difference between the two mean values. The stoichiometry of GFP-Nup was subsequently calculated as I_{Nup}/I_{GFP}.

3. Results

3.1. Single molecule imaging by the spinning disk confocal microscopy

Previously we used glass coverslip adsorbed σ2-GFP as a GFP single molecule intensity standard [17]. A few problems arose during our subsequent usage of this method. First, surface adsorbed σ2-GFP was occasionally observed to dissociate from the glass coverslip surface. The dissociation of GFP molecules can be falsely identified as single-step photobleaching events. Second, σ2-GFP molecules are unevenly distributed on the glass surface which makes it difficult to find an area with appropriately spaced GFP single molecules. Third, there is significant background fluorescence due to the non-specific adsorption of cellular proteins on the glass surface. The background fluorescence reduces the signal-to-noise ratio of single molecule images.

An ideal fluorescence standard should have a layer of appropriately spaced, immobilized and homogenous GFP single molecules on a glass coverslip with minimal adsorption of irrelevant proteins. To that end, we first functionalized the glass surface using nickel nitrilotriacetic acid coupled polyethylene glycol (Ni-NTA-PEG), which is optically transparent and displays very low protein binding or retention. Next, the glass surface was incubated with HEK293 cell lysate expressing 6 × His-GFP. After washing, 6 × His-GFP molecules were specifically immobilized onto the glass surface by the non-covalent binding between Ni-NTA and 6 × His tag. GFP single molecules on the coverslip were imaged under a spinning disk confocal microscope. When coupled with an electron multiplying charge-coupled device (EMCCD) camera, the spinning disk confocal microscope could easily image GFP single molecules (Fig. 1 and Supplementary movie 1). The Ni-NTA-PEG-coated glass surface typically showed dozens of GFP fluorescence spots, which were absent in the control PEG-coated surface (Fig. 1A and B). The background fluorescence of the Ni-NTA-PEG-coated coverslip was minimal but homogenous. Round ROIs (regions of interest) with diameters of 7 pixels were applied to fluorescence objects and the mean fluorescence intensity within each ROI was plotted against time as traces (Fig. 1B–D). During the 2D time-lapse imaging, we observed all-or-none fluorescence intensity or single-step photobleaching, therefore demonstrating that fluorescence objects are GFP single molecules (Fig. 1B–D). The occasional blinking behavior of GFP single molecules was also observed, consistent with the previous report [18]. Those traces not displaying single-step photobleaching were rejected for further analysis as they could represent oligomerized or aggregated 6 × His-GFP. The intensity of a GFP single molecule (I_{GFP}) is acquired by the difference between the mean intensity immediately before and after the photobleaching step. The statistical distribution of I_{GFP} is shown in Fig. 1E. In summary, we have developed a GFP single molecule based fluorescence standard.

Supplementary video related to this article can be found at http://dx.doi.org/10.1016/j.bbrc.2016.09.005.

3.2. Replacement of endogenous Nups by GFP-tagged Nups

Having established the GFP single molecule fluorescence standard, we aimed to quantify the stoichiometry of the NPC in cultured mammalian cells. To reduce the interference of endogenous Nups, we simultaneously co-expressed shRNAs targeting endogenous Nups and corresponding exogenous mutant GFP-Nups. Mutant GFP-Nups harbor silent point mutations that render them insensitive to shRNA-mediated knockdowns. Due to the lack of antibodies against Nups, the silencing effect of shRNAs on endogenous Nup was indirectly assessed by comparing immuno-blots of wild type GFP-Nups in the presence of co-expressed targeting shRNA or control shRNA (shCtrl). shRNAs for Nup35, Nup93, Nup133 and Nup88 typically depleted >50% of co-transfected wild type GFP-Nups (Fig. 2). In all cases, mutant GFP-Nups were resistant to be depleted by corresponding shRNAs. We reasoned that the overexpression of mutant GFP-Nups in combination with the depletion of endogenous copies could ensure a great majority of Nups to be replaced by mutant GFP-Nups.

3.3. Estimation of the stoichiometry of GFP-Nups in the NPC

Under the Nup replacement condition established above, HeLa cells co-expressing mutant GFP-Nups and shCtrl or corresponding targeting shRNAs were processed for imaging using identical conditions as GFP single molecules. Bottom NEs were imaged and typical images of mutant GFP-Nups are shown in Fig. 3A. NPCs were easily resolved as individual objects under our spinning disk

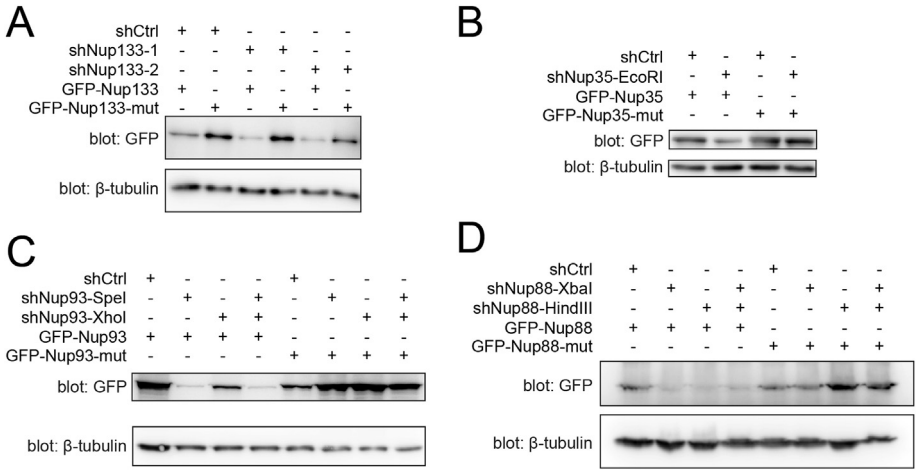

Fig. 2. The replacement of endogenous Nups by GFP-tagged mutant Nups. HeLa cells were transfected with shCtrl or a targeting shRNA and the corresponding wild type or shRNA-resistant mutant GFP-Nup. Cell lysates were blotted by anti-GFP antibody to detect the expressed GFP-Nup. The β-tubulin blot shows equal loading of the cell lysate. Except shNup93-XhoI, all shRNAs showed >50% knockdown of co-expressed wild type GFP-Nups.

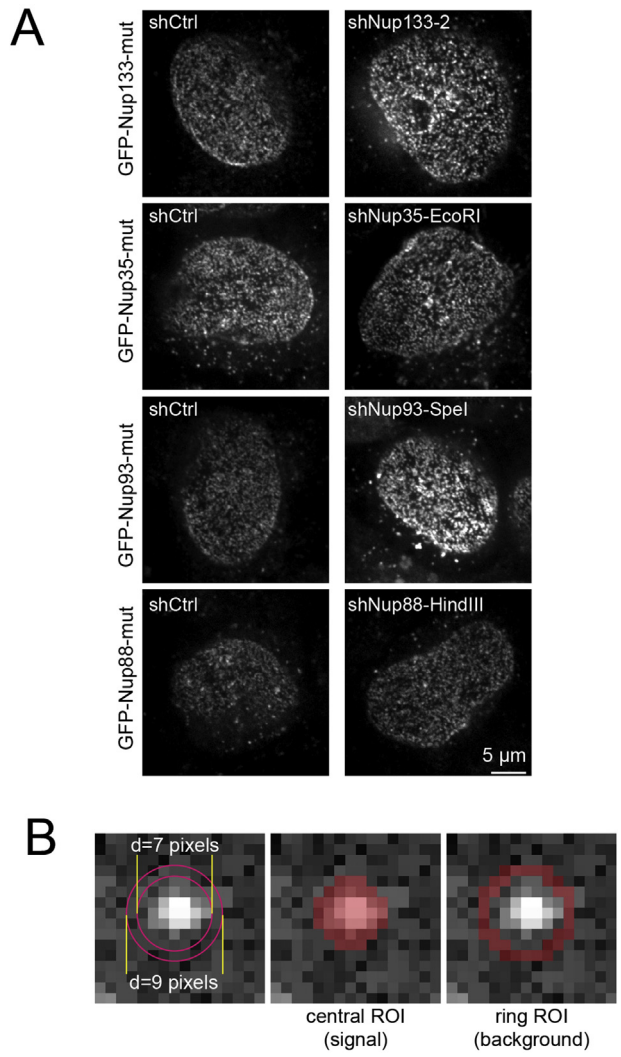

Fig. 3. Representative images of mutant GFP-Nups and the schematic illustration showing the local background subtraction. (A) HeLa cells were transfected with shCtrl or individual shRNA and the corresponding shRNA-resistant mutant GFP-Nup. The image of the bottom NE is shown. Scale bar, 5 μm. (B) The schematic illustration of local background subtraction used in our method. Two concentric round ROIs with diameter of 7 and 9 pixels respectively are drawn around the fluorescence object. The central and ring ROI represent the signal and the local background respectively.

confocal microscope. Care was taken to minimize the photobleaching damages of GFP-Nups. An image stack comprising 3 sections with a z-step of 200 nm was acquired around the bottom of the NE for each GFP-Nup. The section with the best focused NPCs was selected for the subsequent analysis. To correct the uneven background fluorescence intensity on the NE, we adopted the local background subtraction method. As illustrated in Fig. 3B, the mean intensity within the central ROI with a diameter of 7 pixels is contributed by both the NPC and background fluorescence, while that of the ring ROI immediately outside represents the local background fluorescence. The mean intensity of GFP-Nup labeled NPC (I_{Nup}) is therefore obtained by subtracting the mean intensity of the ring ROI from that of the central ROI. The stoichiometry of GFP-Nup was subsequently calculated as I_{Nup}/I_{GFP}, since I_{GFP} was obtained using ROIs of the same size (Fig. 1E). The statistics of measured stoichiometry is listed in Table 1, in which >300 NPCs from 8 to 15 cells were analyzed for each Nup. For Nups with dual targeting shRNAs, the average of the two measured stoichiometry values is used for comparison. Our measured stoichiometry of Nup35, Nup93, Nup133 and Nup88 is 23, 18, 14 and 9, respectively.

4. Discussion

We report here an imaging-based method to quantify the stoichiometry of a protein complex in cultured cells. The feature of our method is the utilization of GFP single molecules as the fluorescence standard in combination with the spinning disk confocal microscope, which is a conventional instrument for cell biology labs. Unlike the total internal reflection fluorescence microscopy based method [4], our method applies to protein complexes located anywhere within a cultured cell. In theory, the stoichiometry of any protein assemblies whose sizes are diffraction-limited or much smaller than the microscope resolution distance (~250 nm) could be quantified by our method. The sizes of many subcellular structures or protein assemblies are within this range, such as cell surface receptor complexes, clathrin-coated pits, ER exit sites, nuclear bodies, kinetochores, virus particles and transport vesicles.

Taking advantage of our newly developed tool, we attempted to measure the stoichiometry of GFP-Nup replaced NPCs in cultured mammalian cells. There are two major factors that could lead to the underestimation of the stoichiometry. First, incomplete replacement of native subunits by GFP-tagged nucleoporins. This was a main problem for the earlier attempt [11]. Our gene replacement protocol should substitute more endogenous Nups but can still be incomplete. Second, the presence of non-fluorescent GFP-Nups in the NPC due to mis-folding, photobleaching, blinking and dark state transition [4]. The stoichiometry of the NPC has recently been systematically studied by fluorescence imaging [5,7,16] and quantitative mass spectrometry [3]. In agreement with Ori et al. [3], our data indicate that the stoichiometry ratio of Nup88, Nup133 and Nup93 is roughly 1:2:2. However, our stoichiometry data is half of values reported by Ori and Finan et al. [3,7]. Our data are different from the report by Mi et al., in which yeast ortholog of Nup88,

Table 1
The stoichiometry or number of mutant GFP-Nups per NPC measured from our study.

Nup complex	Mutant Nup construct	Knockdown shRNA	n	No. of GFP-Nup
Nup93-205 complex	GFP-Nup35-mut	shCtrl	665	19 ± 13
		shNup35-EcoRI	1497	23 ± 12
	GFP-Nup93-mut	shCtrl	516	17 ± 9
		shNup93-SpeI	744	18 ± 8
Nup107-160 complex	GFP-Nup133-mut	shCtrl	453	11 ± 4
		shNup133-1	705	15 ± 6
		shNup133-2	604	13 ± 5
Nup88-214 complex	GFP-Nup88-mut	shCtrl	626	11 ± 6
		shNup88-HindIII	520	8 ± 3
		shNup88-XbaI	625	9 ± 4

HeLa cells were co-transfected with mutant GFP-Nups and corresponding shRNA constructs. NPCs at the bottom of the NE were imaged and quantified for the number of mutant GFP-Nups, which is presented as mean ± standard deviation. n is the number of NPCs that were quantified.

Nup82p, has the same stoichiometry as yeast corresponding orthologs of Nup93 and Nup133 [5]. Considering the 8-fold rotational symmetry of the NPC, our data suggest that the stoichiometry of Nup133 could be 16, consistent with Mi et al. [5] and that of Nup35 and 93 could be 24 and 16 respectively. That the stoichiometry of Nup88 could be 8 is consistent with the copy number of Nup214 which forms a complex with Nup88 [16]. More accurate data could be acquired by further improving the replacement efficiency or genomic GFP-tagging of Nups. It becomes recently known that NPCs are heterogeneous and the stoichiometry of NPCs could be dynamically regulated according to developmental stages of cells [9]. We believe that our method provides a convenient tool to assess the stoichiometry of individual NPCs under a dynamic *in vivo* environment.

Acknowledgements

This work was supported by the following grants to L.L.: NMRC/CBRG/007/2012, MOE AcRF Tier1 RG 48/13, MOE AcRF Tier1 RG132/15 and MOE AcRF Tier2 MOE2015-T2-2-073.

Appendix A. Supplementary data

Supplementary data related to this article can be found at http://dx.doi.org/10.1016/j.bbrc.2016.09.005.

Transparency document

Transparency document related to this article can be found online at http://dx.doi.org/10.1016/j.bbrc.2016.09.005.

References

[1] M.P. Rout, J.D. Aitchison, A. Suprapto, K. Hjertaas, Y. Zhao, B.T. Chait, The yeast nuclear pore complex: composition, architecture, and transport mechanism, J. Cell Biol. 148 (2000) 635–651.
[2] J.M. Cronshaw, A.N. Krutchinsky, W. Zhang, B.T. Chait, M.J. Matunis, Proteomic analysis of the mammalian nuclear pore complex, J. Cell Biol. 158 (2002) 915–927.
[3] A. Ori, N. Banterle, M. Iskar, A. Andres-Pons, C. Escher, H. Khanh Bui, L. Sparks, V. Solis-Mezarino, O. Rinner, P. Bork, E.A. Lemke, M. Beck, Cell type-specific nuclear pores: a case in point for context-dependent stoichiometry of molecular machines, Mol. Syst. Biol. 9 (2013) 648.
[4] M.H. Ulbrich, E.Y. Isacoff, Subunit counting in membrane-bound proteins, Nat. Methods 4 (2007) 319–321.
[5] L. Mi, A. Goryaynov, A. Lindquist, M. Rexach, W. Yang, Quantifying nucleoporin stoichiometry inside single nuclear pore complexes in vivo, Sci. Rep. 5 (2015) 9372.
[6] M. Dundr, J.G. McNally, J. Cohen, T. Misteli, Quantitation of GFP-fusion proteins in single living cells, J. Struct. Biol. 140 (2002) 92–99.
[7] K. Finan, A. Raulf, M. Heilemann, A set of homo-oligomeric standards allows accurate protein counting, Angew. Chem. Int. Ed. Engl. 54 (2015) 12049–12052.
[8] M. Stewart, Molecular mechanism of the nuclear protein import cycle, Nat. Rev. Mol. Cell Biol. 8 (2007) 195–208.
[9] M. Raices, M.A. D'Angelo, Nuclear pore complex composition: a new regulator of tissue-specific and developmental functions, Nat. Rev. Mol. Cell Biol. 13 (2012) 687–699.
[10] E. Hurt, M. Beck, Towards understanding nuclear pore complex architecture and dynamics in the age of integrative structural analysis, Curr. Opin. Cell Biol. 34 (2015) 31–38.
[11] G. Rabut, V. Doye, J. Ellenberg, Mapping the dynamic organization of the nuclear pore complex inside single living cells, Nat. Cell Biol. 6 (2004) 1114–1121.
[12] A. von Appen, J. Kosinski, L. Sparks, A. Ori, A.L. DiGuilio, B. Vollmer, M.T. Mackmull, N. Banterle, L. Parca, P. Kastritis, K. Buczak, S. Mosalaganti, W. Hagen, A. Andres-Pons, E.A. Lemke, P. Bork, W. Antonin, J.S. Glavy, K.H. Bui, M. Beck, In situ structural analysis of the human nuclear pore complex, Nature 526 (2015) 140–143.
[13] T. Stuwe, A.R. Correia, D.H. Lin, M. Paduch, V.T. Lu, A.A. Kossiakoff, A. Hoelz, Nuclear pores. Architecture of the nuclear pore complex coat, Science 347 (2015) 1148–1152.
[14] K.H. Bui, A. von Appen, A.L. DiGuilio, A. Ori, L. Sparks, M.T. Mackmull, T. Bock, W. Hagen, A. Andres-Pons, J.S. Glavy, M. Beck, Integrated structural analysis of the human nuclear pore complex scaffold, Cell 155 (2013) 1233–1243.
[15] M. Eibauer, M. Pellanda, Y. Turgay, A. Dubrovsky, A. Wild, O. Medalia, Structure and gating of the nuclear pore complex, Nat. Commun. 6 (2015) 7532.
[16] M. Schuster, S. Kilaru, P. Ashwin, C. Lin, N.J. Severs, G. Steinberg, Controlled and stochastic retention concentrates dynein at microtubule ends to keep endosomes on track, EMBO J. 30 (2011) 652–664.
[17] L. Lu, M.S. Ladinsky, T. Kirchhausen, Formation of the postmitotic nuclear envelope from extended ER cisternae precedes nuclear pore assembly, J. Cell Biol. 194 (2011) 425–440.
[18] R.M. Dickson, A.B. Cubitt, R.Y. Tsien, W.E. Moerner, On/off blinking and switching behaviour of single molecules of green fluorescent protein, Nature 388 (1997) 355–358.